Mon. Not. R. Astron. Soc. **000**, 1–13 (2002) Printed 12 January 2015 (MN LATEX style file v2.2)

The Variation in Molecular Gas Depletion Time among Nearby Galaxies: What are the Main Parameter Dependencies?

Mei-Ling Huang[1⋆], Guinevere Kauffmann[1]
[1] *Max-Planck Institute for Astrophysics, Karl-Schwarzschild-Str. 1, D-85748 Garching, Germany*

arXiv:1404.7138v2 [astro-ph.GA] 9 Jan 2015

in original form 2014 Jan

ABSTRACT

We re-analyze correlations between global molecular gas depletion time (t_{dep}) and galaxy parameters for nearby galaxies from the COLD GASS survey. We improve on previous work of Saintonge et al. (2011b) by estimating star formation rates (SFRs) using the combination of GALEX FUV and WISE 22 μm data and by deriving t_{dep} within a fixed aperture set by the beam size of gas observation. In our new study we find correlations with much smaller scatter. Dependences of the depletion time on galaxy structural parameters such as stellar surface density and concentration index are now weak or absent. We demonstrate that the *primary* global parameter correlation is between t_{dep} and sSFR; all other remaining correlations can be shown to be induced by this primary dependence. This implies that galaxies with high current-to-past-averaged star formation activity, will drain their molecular gas reservoir sooner. We then analyze t_{dep} on 1-kpc scales in galactic disks using data from the HERACLES survey. There is remarkably good agreement between the global t_{dep}–sSFR relation for the COLD GASS galaxies and that derived for 1 kpc scale grids *in disks*. This leads to the conclusion that the local molecular gas depletion time in galactic disks is dependent on the local fraction of young-to-old stars.

Key words: galaxy formation

1 INTRODUCTION

Numerous studies have attempted to characterize the relation between star formation rate surface density ($\Sigma_{\rm SFR}$) and total gas surface density ($\Sigma_{\rm gas}$). Such relations are often referred to as Kennicutt-Schmidt "laws"(Kennicutt 1998). The Kennicutt-Schmidt "law" is usually expressed as

$$\Sigma_{SFR} \propto \Sigma_{gas}^{N},$$

where $\Sigma_{\rm SFR}$ and $\Sigma_{\rm gas}$ are in units of $M_\odot$ yr^{-1} kpc^{-2} and $M_\odot$ pc^{-2}.

Kennicutt (1998) found N ∼1.4 on global scales for normal and starburst galaxies using Hα as a star formation rate (SFR) indicator and CO and HI line emission as tracers of total cold gas content. It has been demonstrated that this value of N can be explained by gravitational instability: if stars are formed constantly each free-fall time and gas scale height is assumed to be constant, N is equal to 1.5 (e.g., Madore 1977; Elmegreen 1994). Other studies have found values for N that vary in the range between 1 and 3 (see review by Elmegreen 2011). The scatter between different studies is likely due to the fact that a variety of galaxy samples and SFR tracers were used, and that the relation was evaluated over a range of different spatial scales.

Stars form directly in molecular clouds, so the molecular gas, rather than the total or atomic gas, is believed to be linked more directly to the star formation. Wong & Blitz (2002) found a roughly linear correlation between $\Sigma_{\rm SFR}$ and $\Sigma_{\rm H2}$ using Hα and CO observations of 7 gas-rich spirals. In more recent studies, Bigiel et al. (2008) explored the correlation between $\Sigma_{\rm SFR}$ on sub-kpc scales estimated from FUV plus 24 μm fluxes and $\Sigma_{\rm H2}$ derived from CO (J=2-1) line luminosities using a sample of 18 nearby spiral galaxies from the HERACLES project (Leroy et al. 2008). They reported a constant star formation efficiency with depletion time ∼ 2 Gyr among these spirals, independent of local conditions such as orbital timescale, midplane gas pressure and disk stability (Leroy et al. 2008). Their results appeared to suggest that star formation is likely to be a localised process linked only to the local quantity of molecular gas. However, in subsequent work, Momose et al. (2013) found a super-linear Kennicutt-Schmidt law at sub-kpc resolution with slope N

⋆ E-mail: mlhuang@mpa-garching.mpg.de

= 1.3 – 1.8, based on CO (J=1-0) plus Hα and 24 μm data for 10 nearby spiral galaxies. These results would argue that the star formation efficiency in disks depends on local gas surface density. Differences with the published HERACLES results were attributed to the fact that CO(J = 2-1) was used as a tracer of molecular gas mass. If CO(J = 2-1) is enhanced in regions with higher star formation (and hence higher excitation), CO(J = 2-1) may not be a linear tracer of the underlying molecular gas mass.

The COLD GASS project investigated the relation between molecular gas depletion time (t_{dep}) and global galaxy parameters for a representative sample of ∼300 galaxies with stellar masses $10^{10} - 10^{11.5} M_{\odot}$, at redshift 0.02 – 0.05 (Saintonge et al. 2011a). CO(1-0) line measurements were combined with ancillary optical and FUV data from the Sloan Digital Sky Survey (SDSS) and the Galaxy Evolution Explorer (GALEX) satellite to carry out a statistical analysis of global relations between star formation and molecular gas for nearby galaxies (Saintonge et al. 2011b). The global star formation efficiency (SFE) or molecular gas depletion time was found to be dependent on a variety of galaxy parameters, including stellar mass, stellar surface mass density, concentration of the light (i.e. bulge-to-disk ratio), NUV$-r$ colour and specific star formation rate. The strongest dependences were on colour and specific star formation rate.

In subsequent work, Leroy et al. (2013) studied the global Kennicutt-Schmidt law for 30 nearby spirals using CO(2-1) line luminosities as the molecular gas tracer and Hα plus 24μm luminosities as the SFR tracer. They found that all dependences of t_{dep} on global galaxy properties vanished after applying a CO-to-H_2 conversion factor (α_{CO}) that depended on dust-to-gas-ratio. Saintonge et al. (2011b) tested whether there was any relation between t_{dep} and gas-phase metallicity determined from nebular emission lines in their sample and found a null result. Since dust-to-gas ratio and metallicity are well-correlated, this would argue that the explanation given in Leroy et al. (2013) for apparent variations in molecular gas depletion time, cannot be the explanation for the results presented in Saintonge et al. (2011b).

We note that the sample of galaxies studied by Leroy et al. (2013) spans a much narrower range in specific star formation rate than the COLD GASS sample. In particular, massive, bulge-dominated galaxies with low gas fractions and low SFR/M_* are absent. These are the galaxies that contribute most to the observed variations on depletion time (see Figure 7 in Saintonge et al. 2011b).

One hypothesis that has not yet been explored is that different SFR tracers may be the origin of the differing conclusions of Leroy et al. (2013) and Saintonge et al. (2011b). Saintonge et al. (2011b) used spectral energy distribution (SED) fitting technique to derive SFR by fitting UV and optical broad-band photometry to a grid of SED models. Correction for dust extinction was not done directly, but by adopting a set of priors that linked the range of possible values of A_V in the model grid with the NUV-r colours and 4000 Å break strengths of the galaxies. These priors were calibrated using results from the GMACS (Galaxy Multiwavelength Atlas From Combined Surveys) sample (Johnson et al. 2007) , for which accurate star formation rates and extinction measurements could be obtained using UV and far-IR data.

In this paper, we re-derive SFRs for galaxies in the COLD GASS sample by combining GALEX FUV and WISE 22μm data (Wide-field Infrared Survey Explorer;Wright et al. 2010). We thus eliminate the need for statistical dust correction methods. We also improve on the Saintonge et al. (2011b) analysis by measuring molecular gas masses and SFR surface densities within apertures that are exactly matched in radius. We show that not only does this reduce the scatter in our previously derived relations between molecular gas depletion time and galaxy parameters, but also changes some of the scalings. Correlations with galaxy structural parameters such as stellar surface mass density and the concentration index of the light are considerably weakened or entirely absent. We are able to show that the only galaxy parameter that is significantly correlated with the global depletion time of the molecular gas is the ratio of young-to-old stars in the galaxy. We also utilize molecular gas and star formation maps from the HERACLES survey to demonstrate that very similar results are found on sub-kpc scales.

2 DATA

2.1 COLD GASS

2.1.1 Molecular gas and galaxy parameters

Our data set is drawn from the COLD GASS survey catalogue (Saintonge et al. 2011a,b, 2012), which is a subsample of the GASS survey (Catinella et al. 2010). COLD GASS contains CO ($J = 1 - 0$) line measurements from the IRAM 30m telescope for ∼360 nearby galaxies with stellar masses in the range $10^{10} - 10^{11.5} M_{\odot}$ and redshifts in the range $0.025 < z < 0.05$. The reader is referred to Saintonge et al. (2011a) for a detailed description of the sample selection and the observations.

The COLD GASS catalogue also includes global galaxy parameters such as stellar mass, stellar surface mass density, concentration index and NUV-r colour for each targeted galaxy. The first three parameters were taken from the MPA/JHU value-added catalogs (http://www.mpa-garching.mpg.de/SDSS). Stellar masses were calculated by fitting SDSS 5-band optical magnitudes to stellar population synthesis model grids. Stellar surface mass density is defined as $M_*/(2\pi R^2_{50,z})$, where $R_{50,z}$ is the radius containing 50% of the Petrosian flux in the z-band. Concentration index is defined as R_{90}/R_{50} where R_{90} and R_{50} are the radii enclosing 90% and 50% of the total r-band light. The concentration index is well-correlated with the bulge-to-total luminosity ratio of the galaxy (Gadotti et al. 2009; Weinmann et al. 2009). The NUV-r colours of the galaxies were measured using SDSS r-band and GALEX NUV images, which were corrected for Galactic extinction following Wyder et al. (2007).

2.1.2 GALEX FUV and WISE 22μm Data

Instead of adopting the catalog SFRs derived using SED-fitting methods, we derive new SFRs using the combination of FUV emission from GALEX data and mid-infrared 22μm emission from WISE data. FUV emission traces recent unobscured star formation in the galaxy. The missing part of the emission from young, massive stars obscured by surrounding

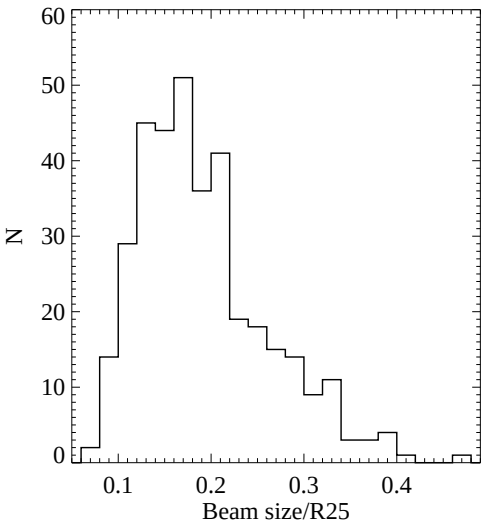

Figure 1. Ratio of IRAM beamsize to R_{25} for galaxies in the COLD GASS sample.

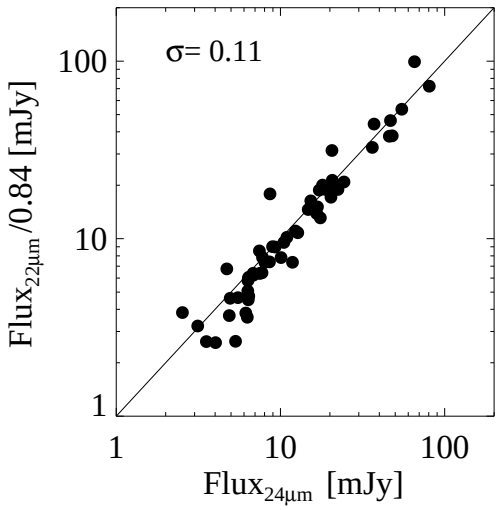

Figure 2. Scaled WISE 22μm fluxes are plotted against Spitzer MIPS 24μm fluxes for galaxies with WISE detections in the GMACS catalog.

dust can be recovered via the measured IR emission, which originates from the dust that is heated by absorbed FUV light.

GALEX provides FUV images with effective wavelength at 1528 Å and angular resolution ∼4.3 arcsec FWHM. We draw the FUV maps from GALEX Data Release 7 products. When several maps from different surveys are available, we select the maps with the longest exposure time. Most of our FUV images are from the Medium Imaging survey (MIS) with typical exposure time ∼1500 seconds; 81 out 366 galaxies only have data from the All-sky Imaging survey (AIS) with typical exposure time ∼100 – 200 seconds. **The limiting flux for MIS is ∼1.4 μJy and for AIS, it is ∼0.2 μJy.** WISE provides 22μm images of the whole sky, with angular resolution 12 arcsec and 5σ point-source sensitivity ∼6mJy. With both GALEX and WISE all-sky maps available, we are able to derive more accurate SFRs for the COLD GASS sample galaxies.

2.2 HERACLES

To compare molecular gas depletion time trends on sub-kpc scales with results obtained globally, we utilize publicly available data from the HERA CO-Line Extragalactic Survey (HERACLES; Leroy et al. 2008). HERACLES has released CO ($J = 2-1$) maps for 48 nearby galaxies, achieving a spatial resolution ∼13 arcsec and an average H_2 surface density detection limit of $\sim 3\ M_\odot pc^{-2}$. For our comparisons with the COLD GASS results , we select 20 massive galaxies with log $(M_*/M_\odot) > 10$ from the catalog in Leroy et al. (2013); these selected galaxies are all located within a distance of ∼ 20 Mpc.

A variety of ancillary data is available for the galaxies we select from HERACLES sample. This includes FUV images from GALEX AIS (four galaxies) and Nearby Galaxy Survey (NGS; Gil de Paz et al. 2007), 24 μm data from the Spitzer Infrared Nearby Galaxies Survey (SINGS; Kennicutt et al. 2003), HI maps from The HI Nearby Galaxies Survey (THINGS; Walter et al. 2008). SINGS provides MIPS 24μm images with an angular resolution ∼6 arcsec and 3 σ sensitivity ∼0.21 MJy sr^{-1}. The maps (natural-weighting) from THINGS have an angular resolution of ∼11 arcsec and are sensitive to $\Sigma_{HI} \geqslant 0.5\ M_\odot\ pc^{-2}$.

The combination of these public datasets enables us to derive gas and SFR surface densities as a function of position in the galaxy by dividing the galaxy into a set of square cells using a 1 kpc^2 grid. Galaxy parameters such as distance, R_{25}, inclination angle, position angle are taken from Leroy et al. (2013). Stellar mass contained within each grid cell is estimated by fitting SDSS 5-band photometry measured for the cell to stellar population models (see sec 3.2).

3 ANALYSES

3.1 Molecular gas depletion time in the COLD GASS sample

Since the IRAM 22″ beam size does not cover the entire optical disk of the galaxies in the COLD GASS sample, aperture corrections were applied to derive total molecular gas masses in Saintonge et al. (2011a). In Fig.1, we plot the ratio of the IRAM beam size to R_{25}, the 25 mag arcsec^{-2} g-band isophotal radius. As can be seen, the beam radius is typically only a quarter of the optical radius. Because the molecular gas is generally quite concentrated towards the center of the galaxy, the corrections to total gas mass are not large *on average* (Saintonge et al 2011a). Nevertheless, when calculating molecular gas depletion time, it is much more accurate to evaluate all quantities within the central 22″ region of the galaxy.

We thus use the observed CO fluxes rather than the corrected CO fluxes from the COLD GASS survey catalogues to

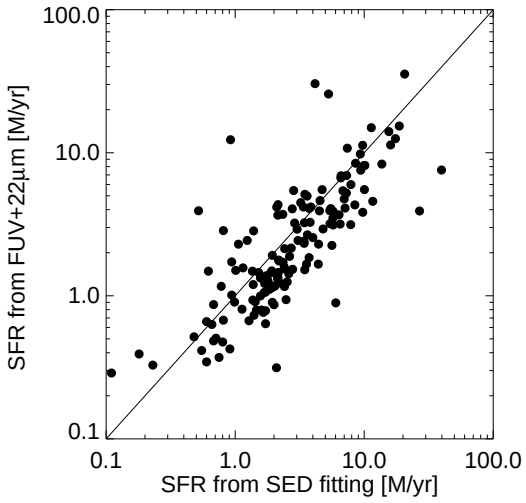

Figure 3. Comparison of SFR estimates from the SED-fitting method presented in Saintonge et al (2011) and the combination of FUV plus 22μm.

derive our estimates of the molecular gas mass. We apply a CO-to-H_2 conversion factor, α_{CO}, in the catalogue to calculate the molecular mass from observed CO line luminosities . In the catalogue, α_{CO} is assumed to have the Galactic value (4.35 $M_\odot$(K km s^{-1} pc^2)$^{-1}$) for the main sample galaxies. For the subset of interacting starburst galaxies with high SFR/M_* values that were added as extra targets towards the end of the program, α_{CO} is assumed to have the "ULIRG" value (1 $M_\odot$(K km s^{-1} pc^2)$^{-1}$). Note that there are only 11 galaxies that require the ULIRG-type α_{CO} in the catalogue. More detailed discussion can be found in Sec 2.3 of Saintonge et al. (2012).

To derive the depletion time, SFR must be estimated within the same region where molecular gas is measured. We place a Gaussian IRAM beam on the FUV and WISE 22 μm maps to derive the central SFR. We note that this was not done in the analysis of Saintonge et al. (2011b), who used total SFR estimates and aperture-corrected CO fluxes. What we want to estimate, is how fast the molecular gas is consumed into stars. To answer this question as accurately as possible, it is clearly preferable that the apertures for the molecular gas and SFR measurements should be closely matched.

We first run SExtractor on the WISE images and mask the detected sources, with the exception of the central target. To remove the background, we first generate the sky image by selecting pixels with values $< 3\ \sigma$ above the median value of the image. We then subtract the median value of the sky image as background. Following Wright et al. (2010) and Jarrett et al. (2011), we apply a colour correction and a flux correction for extremely red sources. Finally, we scale the 22 μm WISE fluxes so that they have the same normalization as the MIPS 24μm fluxes. Using the SED template of normal galaxies from Chary & Elbaz et al. (2001), the flux ratio between WISE 22 μm and Spitzer MIPS 24 μm filters is ∼0.841 at a redshift $z < 0.05$.

One question is whether there is much scatter around this ratio. We use the GMACS catalog from Johnson et al. (2007) to answer this question. The catalogue provides a sample located in two sky regions: the Lockman Hole (part of the Spitzer Wide-area InfraRed Extragalactic survey; SWIRE) and the Spitzer Extra-Galactic First Look Survey (FLS). The median stellar mass of galaxies in this sample is $\mathbf{5{\times}10^{10}}$ $\mathbf{M_\odot}$ and the median redshift is 0.11. The 22μm WISE data is not as deep as SWIRE and FLS surveys, so we only obtain secure 22μm measurements for ∼60 galaxies from the catalogue of Johnson et al. (2007). We predict the fluxes at MIPS-24μm by dividing by 0.84, the value estimated from our single template. The comparison between the pseudo and observed fluxes at Spitzer-24μm is plotted in Fig. 2. As can be seen, the predicted values (y-axis) match the observed values (x-axis) very well and the the scatter is only ∼ 0.11 dex.

Our analysis of the FUV images involves first masking stars and background galaxies using the same procedure applied to the WISE images. We correct for the effects of Galactic extinction using the extinction maps of Schlegel et al. (1998). Finally, we adopt the combined GALEX FUV plus MIPS 24μm relation in Leroy et al. (2008) to estimate the total SFR.

In Fig. 3, we compare the total SFRs derived from FUV plus IR with the SFRs derived via SED-fitting method from the COLD GASS catalogue. There is no significant offset in mean normalization between the two estimates, but there is considerable scatter of around a factor of two. There are 9 galaxies for which the estimates differ by factors of 5-10. Some of these are very dusty galaxies with SFR_{IR}/SFR_{UV} ratios much larger than the average, where SFRs have been underestimated by the SED-fitting method. The galaxies with SFRs overestimated by SED-fitting method have SFR_{IR}/SFR_{UV} ratios close to the mean value, but NUV-r colours that are very red, indicative of old stellar populations.

3.2 HERACLES sample

3.2.1 Calculation of molecular gas depletion time

We follow the procedures outlined in Leroy et al. (2008) and Bigiel et al. (2008) to calculate the molecular gas depletion time in 1-kpc × 1-kpc grid cells. Depletion time in our work is defined as $\Sigma_{H_2}/\Sigma_{SFR}$.

We briefly summarize our steps as follows. We first derive Σ_{H_2} in each 1-kpc grid cell from the reduced HERACLES CO maps adopting the Galactic α_{CO} value, 4.35 $M_\odot$ pc^{-2} (K km s^{-1})$^{-1}$. To derive the Σ_{SFR}, we apply the colour-based masks described in Muñoz-Mateos et al. (2009) to remove stars and background galaxies for the FUV and 24μm images. We check the images again by visual inspection and mask the stars by hand when necessary. We correct the FUV images for Galactic extinction using the maps of Schlegel et al. (1998). All the images are convolved to ∼13″HERACLES resolution using the kernels provided in Aniano et al. (2011). Leroy et al. (2012) pointed out that cirrus emission from old stellar populations could contribute up to ∼ 20% of the total IR luminosity. To remove the cirrus contribution, we apply the method suggested in sec 8.2 of Leroy et al. (2012). **With gas, 24 μm, and FUV data in hand,** they recommended that a first-order cirrus emission

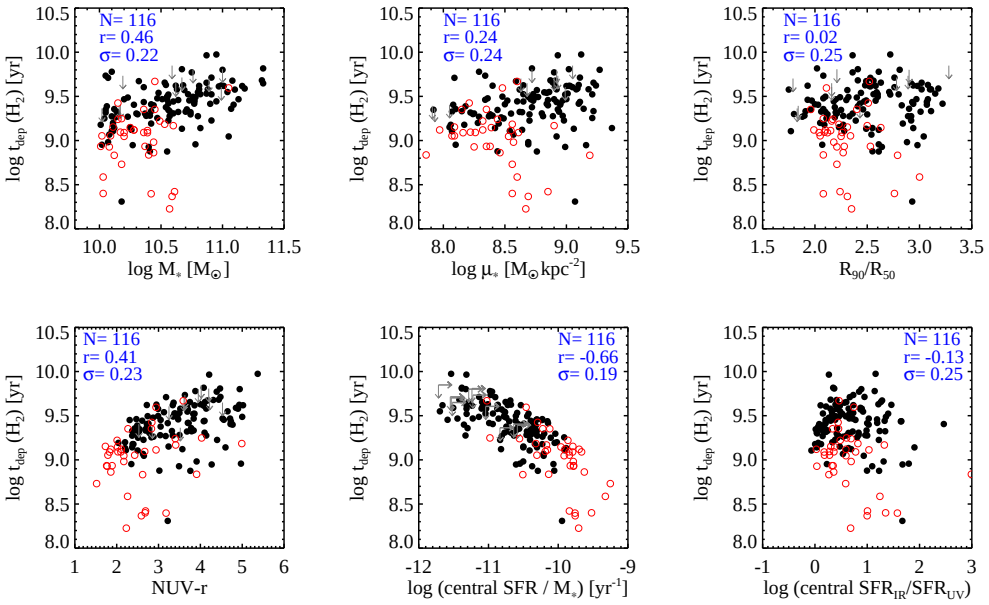

Figure 4. Molecular gas depletion time as a function of global galaxy properties. Black circles denote the representative sample of normal galaxies with secure CO, FUV, and IR measurements. Grey arrows denote the normal galaxies with secure CO detections but upper limits on their SFR estimates. Red circles represent the starburst galaxies. The linear relation is fitted to the normal galaxies with secure measurements of both molecular gas and SFR. N, r, and σ indicate the number of galaxies included in the fit, the Pearson correlation coefficient, and the scatter about the best-fit relation.

Table 1. Summary of the best fit linear relations between t_{dep} and a variety of galaxy parameters for SFR estimates based on SED fitting (cols 4-7) and for SFR estimates based on UV+22μm measurements (cols 8-11). The relations are parametrized as log t_{dep} = m(x-x_0)+b

			SED fitting				UV + IR			
x parameter	Units	x_0	m	b	σ	r	m	b	σ	r
log M_*	log $M_\odot$	10.7	0.40±0.07	9.06±1.03	0.269	0.48	0.33±0.06	9.44±0.02	0.22	0.46
log μ_*	log $M_\odot kpc^{-2}$	8.7	0.40±0.07	8.99±0.88	0.275	0.44	0.17±0.06	9.40±0.02	0.24	0.24
R_{90}/R_{50}	-	2.5	0.37±0.07	8.99±0.22	0.290	0.40	0.01±0.06	9.40±0.02	0.25	0.02
NUV-r	mag	3.5	0.18±0.03	8.98±0.15	0.263	0.49	0.12±0.03	9.41±0.02	0.23	0.41
log SFR/M_*	log yr^{-1}	-10.40	-0.54±0.04	9.06±0.62	0.221	-0.70	-0.37±0.04	9.30±0.02	0.19	-0.66
SFR_{IR}/SFR_{UV}	-	1	-	-	-	-	-0.06±0.05	9.38±0.03	0.25	-0.13

correction could be made using the total gas surface density, i.e. the sum of Σ_{H_2} and Σ_{HI}, where Σ_{HI} is obtained from THINGS data. After we remove this cirrus emission from the 24 μm emission following equation (15) in Leroy et al. (2012), we then adopt their updated calibration coefficient to calculate the SFRs from the linear combination of the FUV and 24 μm luminosities.

We exclude bins with $\Sigma_{SFR} < 10^{-3}$ $M_\odot$ yr^{-1} kpc^{-2} since the calibration becomes poor at very low SFR (Leroy et al. 2012). We also discard the bins with $\Sigma_{H_2} < 3$ $M_\odot$ pc^{-2}, which is the sensitivity limit for the HERACLES CO maps.

3.2.2 Derivation of local parameters

We also derive the local parameters, M_*, stellar mass surface density (μ_*), NUV-r colour, and specific SFR (sSFR) for galaxies in the HERACLES sample. The local parameters are calculated within the 1-kpc scale grids. We measure the SDSS *ugriz* magnitudes and GALEX FUV, NUV magnitudes after we remove stars and correct for Galactic foreground extinction using the methods described above. We use the SED-fitting method in Wang et al. (2011) to derive the stellar mass. **The stellar mass surface density is the stellar mass divided by the physical area of each grid cell , in units of $M_\odot$ kpc^{-2}.** The NUV-r colour is defined as the SDSS *r*-band minus the GALEX NUV magnitude. The parameter, sSFR, is the SFR divided by the stellar mass within each grid cell. We note that M_* = μ_* for 1 kpc square grid cells.

Because Leroy et al. (2013) estimated the stellar mass using 3.6μm fluxes, different from our SED-fitting method, one might worry that this would play a role in our results. As Leroy et al. (2013) provides the global values of M_* estimated from 3.6μm fluxes for the HERACLES sample, we compare our values

with theirs. The linear coefficient is 0.9 with scatter 0.11; we do not see a significant systematic difference.

4 RESULTS

In this section, we present the results of our new derivation of depletion time and we compare with the results of Saintonge et al. (2011b). We also examine the systematic effects that cause the discrepancy between our results and those of the 2011 study. Finally, we show that we can identify a single global galaxy parameter that drives variations in depletion time among different galaxies.

As in Saintonge et al (20011b), the global galaxy parameters that we investigate are M_*, μ_*, R_{90}/R_{50}, NUV-r, and sSFR. In addition, we consider the ratio of the infrared-to-UV flux, IR/UV. The stellar mass, M_*, is an approximate tracer of the global potential well depth of the galaxy. The stellar surface density, μ_*, and the concentration index, R_{90}/R_{50}, are structural parameters. The concentration index is tightly correlated with the bulge-to-disc ratio. The stellar surface mass density is a convenient way of scaling galaxy size and stellar mass and encodes physical information about angular momentum conservation/loss during the process of galaxy formation. The global NUV-r colour is a measure of the ratio of young stars that are not obscured by dust to older stars. The sSFR parameter is the ratio of the current star formation rate, corrected for dust extinction, to the total stellar mass. For consistency, we derive sSFR within the same 22″area of the galaxy where we measure the molecular gas mass. The ratio of the total IR to FUV luminosity is a robust estimate of the dust attenuation (e.g., Gordon et al. 2000; Bell 2003; Hao et al. 2011). Although we do not have enough multi-wavelength data to estimate the total IR luminosity, the 24μm luminosity has been shown to correlate linearly with the total IR luminosity (Wu et al. 2005; Calzetti et al. 2007; Rieke et al. 2009). Thus, we use the ratio of the $SFR_{22\mu m}$ to SFR_{FUV} (IR/UV) as our indicator of dust attenuation.

4.1 Depletion time based on our new SFR estimates

We plot depletion time results based on our new SFR estimates as a function of global physical properties of galaxies in Fig.4. The black circles show galaxies in the representative sample with secure CO, FUV and 22μm detections. The grey arrows show galaxies with secure CO detections but with SFR upper limits. An extra set of galaxies with high values of SFR/M_* were observed at the end of the COLD GASS program in order to extend the dynamic range in star formation probed by the observations. We will refer to these galaxies as "starburst" systems and we indicate them as red symbols on the figure. Some of these galaxies have enhanced infrared luminosity and dust temperature and we thus use the "ULIRG" value of α_{co} ($1\ M_\odot\ pc^{-2}\ (K\ km\ s^{-1})^{-1}$) to derive their molecular gas masses. We note that some of these starburst galaxies are interacting/merging systems and it is inevitable to include emission from their companions when we calculate their global properties. To minimize any confusion, we visually identify eight interacting/merging systems and exclude them in the following analyses and discussions. We perform linear fits to galaxies from the representative sample only and the number of galaxies in the sample (N), the Pearson linear correlation coefficient (r), and the scatter (σ) are indicated on the figure.

Our new linear relations are compared with those derived by Saintonge et al. (2011b) in Table 1. Three main changes can be seen:

(i) The normalization b changes. The resulting depletion times are a factor of two longer than quoted in Saintonge et al. (2011b) and now agree very well with HERACLES results (see later). The change in normalization occurs because the apertures within which we measure the molecular gas and the SFR are now well-matched.

(ii) The scatter σ in the relations between depletion time and global galaxy parameters is significantly reduced. This occurs for all the relations and is a consequence of our improved star formation rate estimates, which do not have to be corrected for dust in a statistical fashion.

(iii) The slopes of the relations between depletion time and the structural parameters, μ_* and concentration index R_{90}/R_{50}, are significantly flatter than before. In particular, there is now no correlation at all between depletion time and galaxy bulge-to-disk ratio, whereas Saintonge et al. (2011b) found a very significant correlation.

There are still strong correlations between the depletion time and stellar mass, NUV-r color and sSFR, with only small changes in slope from previously. We note that the depletion time is not dependent on the IR/UV ratio. In the next section, we investigate the systematic effects in the dust extinction properties of the galaxies, which are the main cause of the discrepancy between our work and that of Saintonge et al. (2011b).

4.2 Systematic effects caused by dust attenuation

In Fig. 5, we illustrate how the correlation coefficients r and the scatter σ about the best-fit linear relation between molecular gas depletion time and galaxy properties change when we derive star formation rate purely from the UV flux (SFR_{UV}), purely from the IR flux (SFR_{IR}) and from the sum of the two (SFR_{UV+IR}). The bar plots show the value of σ, as indicated on the left-hand axis; the solid circles show the correlation coefficients, as indicated on the right-hand axis. We first observe that the scatter tends to be significantly larger for the UV-based relations, and of comparable magnitude for IR and UV+IR-based relations. The strength of the correlations with the structural parameters μ_* and R_{90}/R_{50} is only strong for the UV-based relations, and largely disappears for the SFR_{IR} and SFR_{UV+IR} relations. In contrast, the strength of the correlations with stellar mass M_* and specific star formation rate SFR/M_* are the same for SFR_{UV}, SFR_{IR} and SFR_{UV+IR}. This supports our conjecture that systematics in IR/UV ratio (or dust extinction) are the main reason for the changes between the results presented in this paper and those in Saintonge et al. (2011b).

As both t_{dep} and IR/UV include the UV flux, it is worth using an independent estimate of dust extinction to investigate the effect of dust systematics on our results. A subsample of the COLD GASS galaxies have long-slit spectra

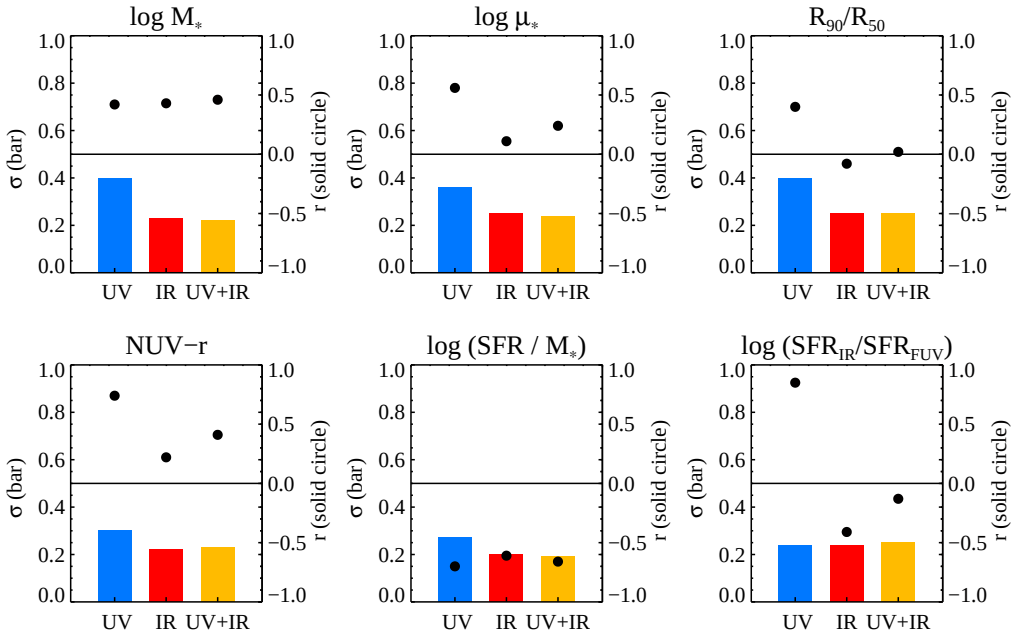

Figure 5. The scatter (σ) and the correlation coefficient (r) of the fitted linear relations between depletion time and galaxy parameters based on 3 different SFR tracers: UV+IR, IR, FUV. The bar plots show the value of the scatter as indicated on the left y-axis; the solid circles denote the correlation coefficients as indicated on the right y-axis.

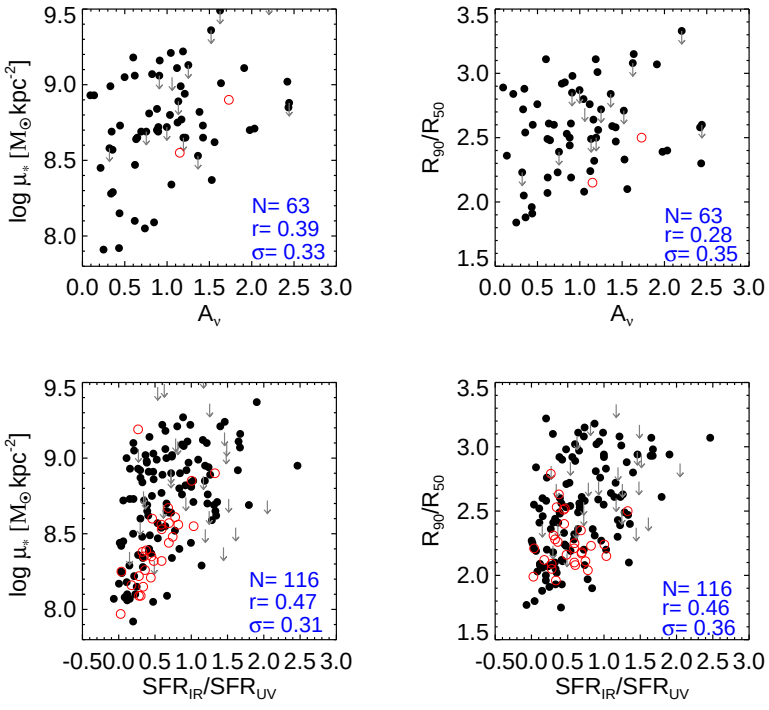

Figure 6. Stellar surface density and concentration index as functions of Aν and IR/UV.

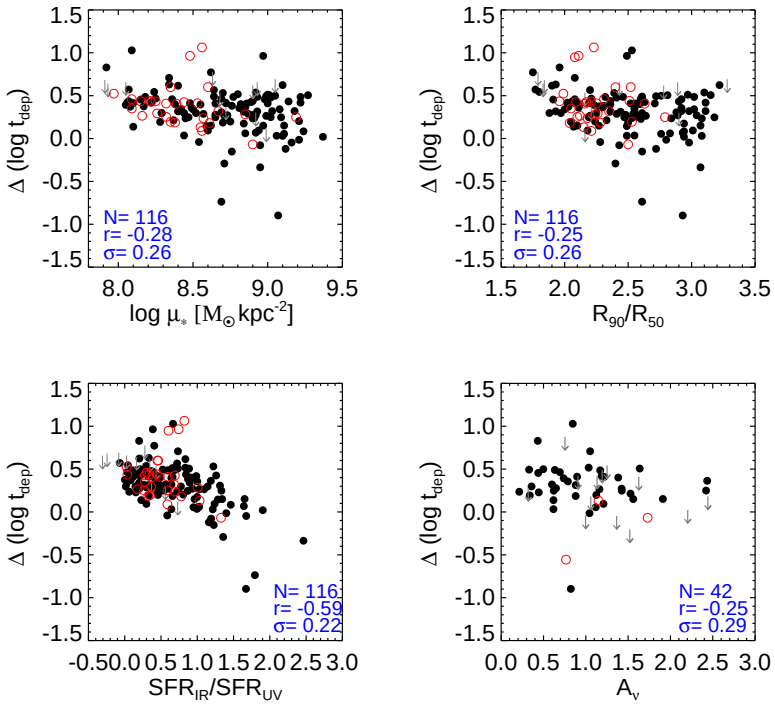

Figure 7. Difference in the depletion time , Δ (log t_{dep}), measured in Saintonge et al. (2011b) and our work as functions of stellar surface density, concentration, IR/UV ratio and dust extinction.

along their major axes (Moran et al. 2012), from which we can calculate the extinction A_ν from the Balmer decrement, $L(H_\alpha)/L(H_\beta)$. The spectra were spatially binned outward from the galaxy center to ensure an adequate S/N in every bin. We exclude the bins with low S/N for the Balmer lines and weight the bins with reliable measurements by the stellar mass contained within the annulus spanned by the bin boundaries, to get a representative A_ν value for the whole galaxy.

In Fig. 6, we plot μ_* and R_{90}/R_{50} as a function of A_ν and the IR/UV ratio. These structural parameters correlate strongly with both A_ν and IR/UV. In order to ascertain whether these correlations are responsible for differences in our depletion time results with respect to those of Saintonge et al (2011b), we calculate the difference between the two depletion time estimates Δ log (t_{dep})= log t_{dep} (this paper) − log t_{dep} (Saintonge et al. 2011b). In Fig. 7, Δ log (t_{dep}) is plotted against μ_*, R_{90}/R_{50}, IR/UV, and A_ν. As can be seen, our depletion time estimates become shorter with respect to those in Saintonge et al. (2011b) when galaxies have higher stellar surface densities and larger concentration indices. The difference Δ log (t_{dep}) is also correlated with IR/UV and A_ν.

4.3 Primary or Induced Correlation?

Our results show that molecular gas depletion time is strongly correlated with M_*, NUV-r and sSFR, and is more weakly correlated with μ_*. One question is whether these correlations are independent of each other. Almost all global galaxy parameters correlate strongly with stellar mass, so one might expect the molecular gas depletion time to correlate with M_* even if the *primary* correlation is with some other parameter. In this section, we attempt to separate primary and induced correlations through analysis of residuals. We note that NUV-r and sSFR have similar physical meaning in that they both serve as an indicator of the ratio of young-to-old stars in the galaxy, so for simplicity we only consider sSFR, which does not depend on dust extinction.

We fit a linear relation to the t_{dep} versus M_* relation and ask whether the residuals of t_{dep} from this relation are correlated with sSFR. Similarly, we also fit a linear function to the t_{dep}–sSFR relation and examine if the residuals correlate with M_*. The results are shown in Fig. 8. The blue line shows the fit to the representative sample, while the red line shows the fit to the combination of normal and starburst galaxies. The residuals are measured with respect to the blue line.

As seen in the lower panel of Fig. 8, the residuals from the t_{dep}–M_* relation correlate strongly with sSFR, while the residuals from the t_{dep}–sSFR relation correlate very weakly with M_*. We note that there is one galaxy with particularly low depletion time (0.1 Gyr) and with a central sSFR $\sim 10^{-9.9}$ yr^{-1}, which causes most of this weak correlation. In the MPA-JHU catalog, this galaxy has been classified as a galaxy with an AGN in the center. If this galaxy is excluded, there is no longer any significant correlation between the t_{dep} residuals and stellar mass.

We carry out the same exercise for the relation between t_{dep} and μ_*. The results are plotted in Fig. 9. The residuals of the t_{dep}–μ_* relation are strongly correlated with sSFR, with a significance r =−0.58. By contrast, there is no relation

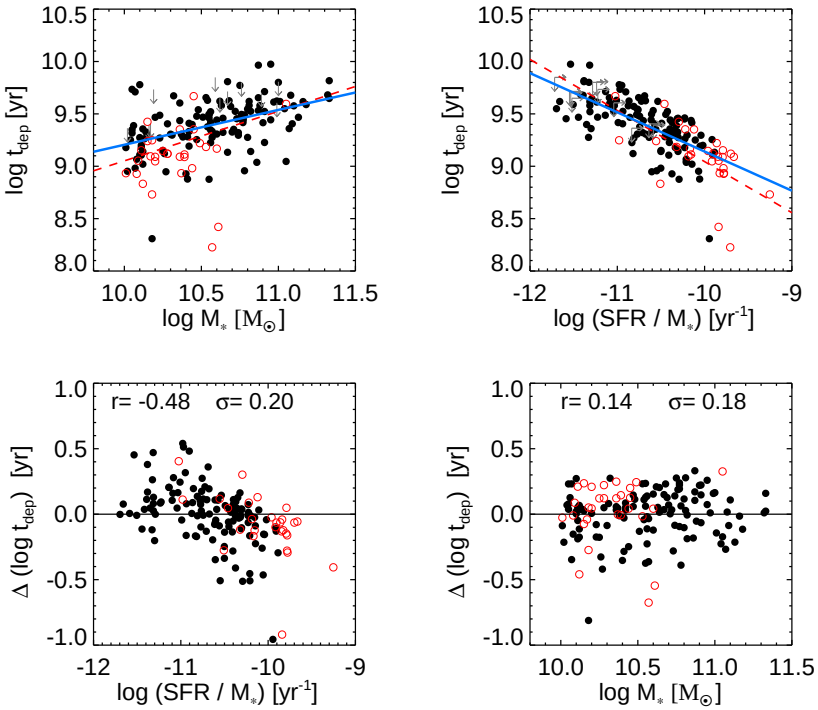

Figure 8. Upper panels: molecular gas depletion time is plotted as a function of M_* and SFR/M_*. Blue lines show the best-fit linear relation for galaxies in the representative sample, while the red lines show the best-fit linear relation for the sample that includes the starburst systems. Bottom left : The residuals from the best fit $t_{dep} - M_*$ relation are plotted as a function of SFR/M_*. Bottom right: The residuals from the best fit $t_{dep} - SFR/M_*$ relation are plotted as a function of M_*.

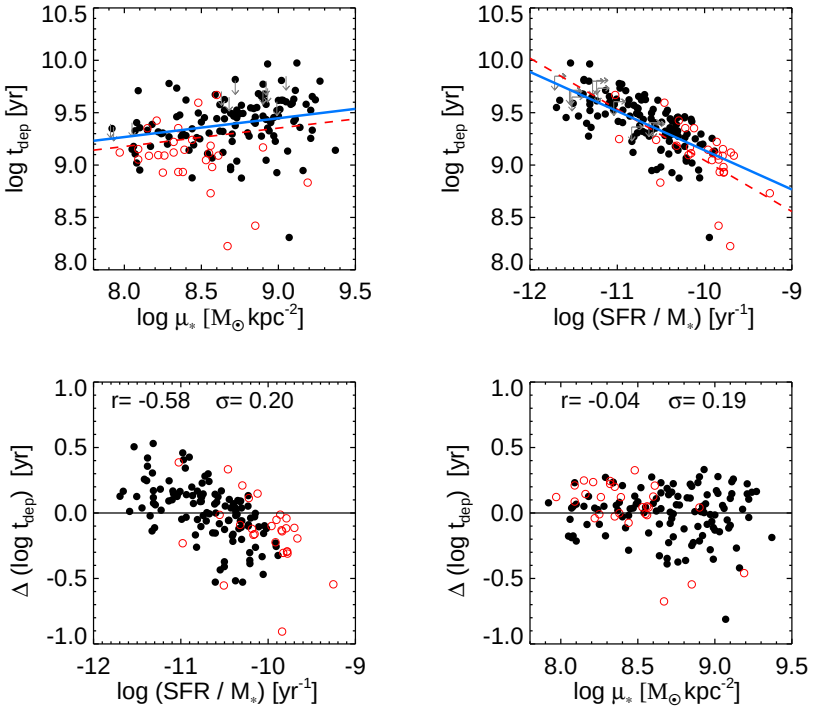

Figure 9. As in Figure 8, except that M_* has been replaced by μ_*

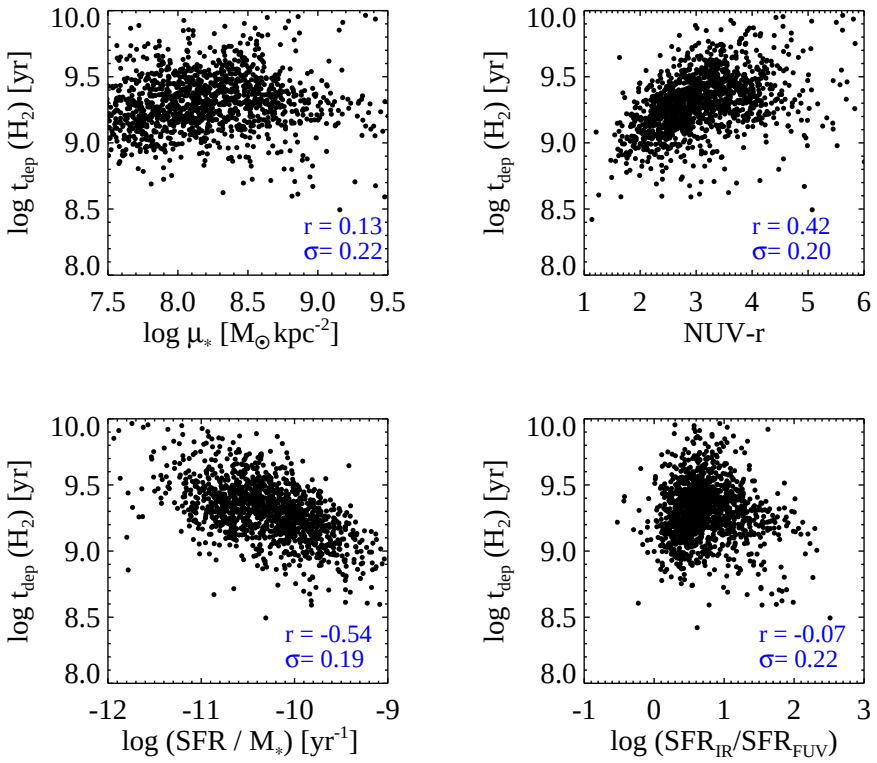

Figure 10. Molecular gas depletion times evaluated within 1kpc^2 area grid cells as functions of stellar surface density, NUV-r color, sSFR and IR/UV for galaxies from the HERACLES sample.

Table 2. Summary of the best-fit linear relations between t_{dep} and local parameters for grid scale data from the HERACLES sample. The relations are parametrized as log t_{dep} = m(x-x$_0$)+b

x parameter	Units	x$_0$	m	b	σ	r
log μ_*	log M$_\odot$kpc^{-2}	8.7	0.06±0.01	9.33±0.01	0.22	0.13
NUV-r	mag	3.5	0.12±0.0 1	9.35±0.01	0.20	0.42
log SFR/M$_*$	log yr^{-1}	-10.40	-0.24±0.01	9.32±0.01	0.19	-0.54
SFR$_{IR}$/SFR$_{UV}$	-	1	-0.04±0.01	9.29±0.01	0.22	-0.07

between μ_* and the residuals of the t_{dep}–sSFR relation. We again conclude that the primary relation is the one between t_{dep} and sSFR.

The trend of t_{dep} with sSFR on global scale can be also seen in the results based on a fixed α_{CO} from Leroy et al. (2013). In their Table 6, the rank coefficient (1st column) for t_{dep}–sSFR relation is -0.38 **for all sample and** -0.27 **for the sample with log M$_*$ > 10. This indicates there is a dependence of t_{dep} on sSFR though this dependence is weaker than our finding. This might be due to differences in the sample size and the range of the galaxy properties, as discussed in Sec 1.**

4.4 Comparison with results for 1 kpc grids

In order to examine whether the trends we find in the COLD GASS sample are similar to those found on smaller (1 kpc) scales, we utilize data from the HERACLES project. We derive depletion time on grids with 1 kpc^2 area and study the dependence on local physical properties, such as stellar surface density, NUV-r color, sSFR, and IR/UV ratio. As discussed in section 3.2, **bins with low SFR surface densities are excluded** and we also remove the IR cirrus emission from old stellar populations following the procedures outlined in Leroy et al. (2012).

We plot the molecular gas depletion time versus stellar surface mass density, NUV-r color, sSFR, and IR/UV ratio in Fig. 10. As in the COLD GASS sample, the depletion time on 1 kpc grid scales in the HERACLES sample is strongly correlated with NUV-r and sSFR, but does not show significant dependence on the local stellar mass density or the IR/UV ratio.

To quantify the strength of the correlations on local scales, we also fit linear relations to the HERACLES data and summarize the parameters of the best-fit relations in

Table 2. Generally, the slopes and the correlation coefficients are somewhat lower for the grid measurements compared to the COLD GASS sample. The slope and the significance of the t_{dep}–sSFR correlation on grid scales are −0.24 and −0.54, compared to −0.37 and −0.66 on global scales.

We plot the t_{dep}–sSFR relations for grid and global scales, as well as the best-fit linear relations, in Fig. 11. We separate the grid cells into those located in the bulge-dominated and disk-dominated regions of galaxies as follows. We apply the GALFIT code (Peng et al. 2010) to the SDSS r-band images to decompose galaxies into bulges and disks. To fit the luminosity profile of the galaxies, the code assumes a two-component model, Sersic bulge plus Sersic disk profile, where the Sersic n values for the bulge and disk are allowed to vary from 1.5 to 4 and from 0.8 to 1.2, respectively.

Two main conclusions emerge from the results shown in Fig. 11: a) the global t_{dep}–sSFR relation for the COLD GAS galaxies overlaps that for the *disk grid cells* quite well. b) The number of grid cells in bulge-dominated regions is quite low. Some of these bulge grid cells do fall below the fitting relation. This is consistent with the results in Leroy et al. (2013), where shorter molecular gas depletion time were found in the nuclear nuclear regions of some galaxies. Nevertheless, it is quite clear from Fig. 11 that the main t_{dep}–sSFR correlation is driven by disk-dominated regions of the galaxy.

Because the SFR estimate is included in the calculation of both t_{dep} and sSFR, one might worry that the correlation between t_{dep} and sSFR might be induced rather than a real correlation. This issue was addressed in detail in Saintonge et al. (2011b). It was demonstrated that molecular gas depletion time correlated very well with 4000 Å break strength measured from the SDSS fiber spectrum, which provides an independent estimate of the ratio of young-to-old stars in the galaxy. In addition, these authors carried out Monte Carlo simulations where they showed that the observed relation was too strong to be "induced" by scatter arising from measurement errors.

In Fig. 12, we investigate whether the depletion time has dependence on the molecular gas surface density, Σ_{H_2} and the molecular gas surface density scaled by the stellar mass within the grid cell, Σ_{H_2}/M_*. As can be seen, there is no dependence of t_{dep} on Σ_{H_2}. However, when Σ_{H_2} is scaled by the stellar mass measured in the grid cell, a mild dependence on Σ_{H_2}/M_*, with the linear coefficient r = −0.11, is found. **This result might indicate that the *local density of evolved stars has an effect on the molecular gas depletion time.***

We conclude that molecular gas is depleted most quickly in regions of the galaxy where the current star formation rate is high and the density of already-formed stars is low. This may be true in spiral arm regions – this is a hypothesis that we will investigate in a future paper.

5 SUMMARY AND DISCUSSION

In this paper, we re-analyze the relations between global molecular gas depletion time and a variety of galaxy parameters for nearby galaxies from the COLD GASS survey with stellar masses in the range 10^{10} – $10^{11.5}$ $M_\odot$ and redshifts in the range 0.02.– 0.05. The molecular gas mass

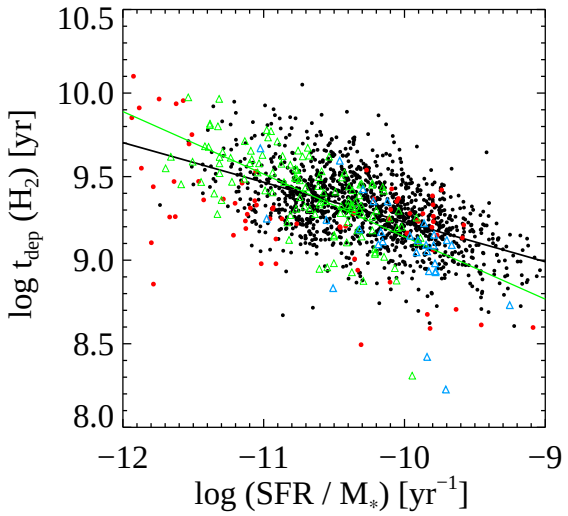

Figure 11. Comparison of the global t_{dep}–sSFR relation for COLD GASS galaxies and for measurements on 1 kpc grid scales for galaxies in the HERACLES sample. Green and blue triangles denote the representative and starburst samples from the COLD GASS survey. Black and red points denote the grid measurements in *disc* and *bulge* regions of galaxies from the HERACLES sample. Linear relations are fit to both the COLD GASS representative sample (green line) and the HERACLES data (black line).

is estimated from the CO(J=1-0) line measurements and our updated estimates of star formations use the combination of GALEX FUV and WISE 22 μm data. In agreement with Saintonge et al. (2011b), we find that the molecular gas depletion time depends strongly on galaxy stellar mass, NUV-r colour and sSFR. Our results differ from those in Saintonge et al. (2011b) in that we find that the dependences of the depletion time on galaxy structural parameters such as stellar surface density and concentration index, are weak or absent. We demonstrate that the differences with the Saintonge et al. (2011b) analysis arise from the fact that dust extinction as measured by the ratio of 22 micron to far-UV flux in the galaxy, correlates strongly with μ_* and concentration. We further demonstrate that the dependence of t_{dep} on M_* is actually driven by the primary correlation between t_{dep} and sSFR.

We compare our results with molecular gas depletion time estimates on 1-kpc scales using publicly available data from the HERACLES survey. We find remarkably good agreement with our global t_{dep} versus sSFR relation. On sub-galactic scales, we are able to ascertain that t_{dep} is not correlated with Σ_{H_2}, but is weakly correlated with Σ_{H_2}/M_*, indicating that the presence of old stars has an effect on the ability of molecular clouds to form new stars.

We note that the parameter, sSFR, is the ratio of current SFR to the stellar mass built up by the past star formation. The strong correlation between t_{dep} and sSFR, extending over a factor of 10 in t_{dep} in our sample, leads to the inference that the molecular gas depletion time is dependent on the star formation history of the galaxies. Those galaxies with high current-to-past averaged star formation activity, will drain their molecular gas reservoir sooner.

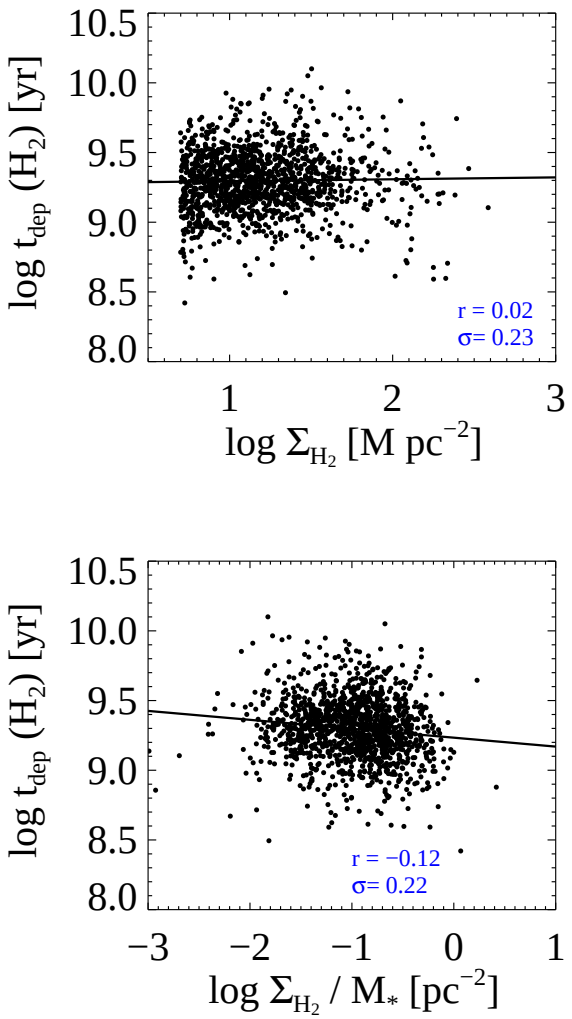

Figure 12. Depletion time as a function of molecular gas surface density and molecular gas surface density per unit stellar mass for the HERACLES grid measurements.

The influence of metallicity on α_{CO} value is always a concern whenever the star-formation law is studied. One might question whether our assumption of a fixed α_{CO} value is appropriate. Sandstrom et al. (2013) studied variations in α_{CO} using a subset of 26 galaxies from the HERACLES sample. They showed that metallicity effects on α_{co} are very weak over the metallicity range spanned by the HERACLES disc galaxies. α_{co} has been shown to depart significantly from the typical Galactic value only below a metallicity $\sim$ 1/3 – 1/2 solar (e.g., Glover & Mac Low 2011; Leroy et al. 2011; Bolatto et al. 2013). We would also expect to see a dependence of gas depletion time on the dust content of the galaxy, if our results were simply a consequence of variations in α_{CO}. From Fig. 4 and 10, we know that the depletion time on both global and local scales does not show any correlation with IR/UV ratio.

Sandstrom et al. (2013) did find that α_{CO} is dependent on other galaxy parameters, such as average radiation field intensity, PAH fraction, stellar mass surface density, SFR surface density and dust mass surface density. The α_{CO} value appears to decrease as the stellar mass and SFR surface densities increase. We note that these two effects cancel when we derive sSFR. We conclude that it is unlikely that the small variations in α_{CO} found by Sandstrom et al. (2013) explain our observed relation between t_{dep} and sSFR.

In future work, we will investigate whether the strong t_{dep}–sSFR is connected to the structure of the interstellar medium, such as the presence of spiral arms. Gas clouds are compressed in spiral arm regions and one might hypothesize that galaxies with high SFR/M_* might have more arm structures than those with low SFR/M_*, leading to the observed variation in molecular depletion time scales in disks.

ACKNOWLEDGMENTS

We thank Amélie Saintonge, Jing Wang, Richard D'Souza, Jarle Brinchmann, Sambit Roychowdhury, Li Shao and Frank Bigiel for helpful discussions.

GALEX is a NASA Small Explorer, launched in 2003 April, developed in cooperation with the Centre National dEtudes Spatiales of France and the Korean Ministry of Science and Technology.

This publication makes use of data products from the Wide-field Infrared Survey Explorer, which is a joint project of the University of California, Los Angeles, and the Jet Propulsion Laboratory/California Institute of Technology, funded by the National Aeronautics and Space Administration.

Funding for the SDSS and SDSS-II has been provided by the Alfred P. Sloan Foundation, the Participating Institutions, the National Science Foundation, the US Department of Energy, the National Aeronautics and Space Administration, the Japanese Monbukagakusho, the Max Planck Society, and the Higher Education Funding Council for England. The SDSS is managed by the Astrophysical Research Consortium for the Participating Institutions. The Participating Institutions are the American Museum of Natural History, Astrophysical Institute Potsdam, University of Basel, Cambridge University, Case Western Reserve University, University of Chicago, Drexel University, Fermi National Accelerator Laboratory, the Institute for Advanced Study, the Japan Participation Group, Johns Hopkins University, the Joint Institute for Nuclear Astrophysics, the Kavli Institute for Particle Astrophysics and Cosmology, the Korean Scientist Group, The Chinese Academy of Sciences (LAMOST), the Leibniz Institute for Astrophysics, Los Alamos National Laboratory, the Max-Planck-Institute for Astronomy (MPIA), the Max-Planck-Institute for Astrophysics (MPA), New Mexico State University, Ohio State University, University of Pittsburgh, University of Portsmouth, Princeton University, the US Naval Observatory and the University of Washington.

REFERENCES

Aniano G., Draine B. T., Gordon K. D., Sandstrom K., 2011, PASP, 123, 1218

Bolatto A. D., Wolfire M., Leroy A. K. 2013, ARA&A, 51, 207
Bell E. F., 2003, ApJ, 586, 794
Calzetti D. et al., 2007,ApJ, 666, 870
Catinella B. et al., 2010, MNRAS, 403, 683
Bigiel F., Leroy A. K., Walter F., Brinks E., De Blok W. J. G., Madore B., Thornley M. D., 2008, ApJ, 136, 2846
Bigiel F. et al., 2011, ApJL, 730, L13
Chary R., Elbaz D., 2001, ApJ, 556, 562
Elmegreen B. G., 1994, ApJ, 425, L73
Elmegreen B. G., 2011, preprint (arXiv:1101.3108)
Gadotti D. A. et al., 2009, MNRAS, 393, 1531
Gil de Paz A. et al., 2007, ApJS, 173, 185
Glover S. C. O., Mac Low M.-M., 2011, MNRAS, 412, 337
Gordon K. D., Clayton G. C., Witt A. N., Misselt K. A. ,2000, ApJ, 533, 236
Hao C.-N., Kenicutt R. C. Jr., Johnson B. D., Calzetti D., Dale D. A., Moustakas J. ,2011, ApJ, 741, 124
Jarrett T. H. et al., 2011, ApJ, 735,112
Johnson B. D. et al., 2007, ApJS, 173,377
Kennicutt R. C. Jr., 1998, ARA&A, 36, 189
Kennicutt R. C. Jr. et al., 2003, PASP, 115, 928
Leroy A.K. et al., 2008, ApJ, 136, 2782
Leroy A.K. et al., 2011, ApJ, 737,12
Leroy A.K. et al., 2012, ApJ, 144,3
Leroy A.K. et al., 2013, ApJ, 146,19
Madore B. F., 1977, MNRAS, 178,1
Moran S. M. et al., 2012, ApJ, 745, 66
Muñoz-Mateos et al., 2009, ApJ, 703,1569
Momose R. et al., 2013, ApJL, 772, L13
Peng C. Y., Ho L. C., Impey C. D., Rix H.-W. et al., 2010, MNRAS, AJ, 139, 2097
Rieke G. H. et al., 2009, ApJ, 692, 556
Saintonge A. et al., 2011a, MNRAS, 415, 32
Saintonge A. et al., 2011b, MNRAS, 415, 61
Saintonge A. et al., 2012, ApJ, 758, 73
Sandstrom K. M. et al., 2013, ApJ,777,5
Schlegel D. J., Finkbeiner D. P., Davis M., 1998, ApJ, 500,525
Walter F., Brinks E., de Blok W. J. G., Bigiel F., Kennicutt R. C. Jr., Thornley M. D., Leroy A. K., 2008, AJ, 136, 2563
Wang J. et al., 2011, MNRAS, 412, 1081
Weinmann S. M., Kauffmann G., van den Bosch F. C., Pasquali A., McIntosh D. H., Mo H., Yang X., Guo Y., 2009, MNRAS, 394, 1213
Wong T., Blitz L., 2002, ApJ, 569, 157
Wright E. L. et al., 2010, AJ, 140, 1868
Wu J. et al., 2005, ApJ, 635L, 173
Wyder T. K. et al., 2007, ApJS, 173, 293